



Wide ASPECS



THESIS

submitted in partial fulfillment of the
requirements for the degree of

MASTER OF SCIENCE
in
ASTRONOMY

Author : Jacob Bieker
Student ID : 2153246
Supervisor : Prof. Jacqueline Hodge
2nd corrector : use \corrector{...} to define

Leiden, The Netherlands, June 30, 2019

Wide ASPECS

Jacob Bieker

Leiden Observatory, Leiden University
P.O. Box 9513, 2300 RA Leiden, The Netherlands

June 30, 2019

Abstract

In this research, data from the Wide ASPECS survey is used to look at the clustering and properties of blindly selected CO emitters within the GOODS-South region of the sky. The frequency range covered enables the identification of CO emission lines up to a $z = 4.4$. The survey builds on the results of the ASPECS Pilot and Large Program surveys, with 35 potential CO line candidates found, and 3 lines matched with counterparts. The properties of these counterparts are examined to determine the physical properties of CO emitters within the field. There is clear increase in the two-point correlation function at higher fidelities for the CO line candidates, suggesting that there are real sources present, although the results are quite noisy. A comparison of the r_0 for these CO sources to the r_0 for other populations of galaxies is performed. These results build toward calculating the first direct constraints on the clustering bias of CO emitters, and therefore their halo mass.

Contents

1	Introduction	1
1.1	Creating Galaxies	1
1.2	Observing Galaxies	2
1.3	From Observations to Models	3
1.4	Galaxies in Groups	3
2	Spectral Line Survey	5
2.1	Previous Work	5
2.2	This Survey	6
2.2.1	Ancillary Data	7
2.2.2	SED Fitting	9
2.3	Method	9
2.3.1	Line Search and Fidelity	11
2.3.2	Cross-matching and Redshift Determination	12
2.4	Results	14
2.4.1	Catalog	15
2.5	Discussion	15
3	Clustering	19
3.1	Previous Work	19
3.2	Method	19
3.2.1	Angular Correlation Function	19
3.2.2	Obtaining r_0 and γ	20
3.3	Results	21
3.4	Discussion	25
4	Conclusion	27
4.1	Future Work	27

Introduction



Gas is the building block of stars and galaxies, and molecular gas in the interstellar medium (ISM) is the fuel for star formation [1]. This gas can inform us about the evolution of galaxies and large scale structure in the universe, especially as observations cover larger and larger volumes of space. Using radio and submm telescopes, such as the Atacama Large Millimeter/submillimeter Array (ALMA), this gas can be observed through looking for the transition lines of carbon monoxide (CO). In the Wide ALMA Spectroscopic Survey in the Hubble Ultra Deep Field (Wide ASPECS) survey, ALMA has been used to observe the largest volume of space yet for CO emissions, on the order of 550,000 cMpc. This enables the ability to look at these CO emitters in bulk for the first time.

This project is focused on using Wide ASPECS to estimate the properties of CO emitters, and to determine the spatial density of CO emitters. Building upon the success of the previous ASPECS Pilot and Large Program surveys [1, 2], this research also works to cross-match detected CO lines with galaxies present in the survey volume, and builds the basis for future work with this data on constraining the CO luminosity function, the cosmic density of molecular gas in galaxies $\rho(H_2)$, and the clustering bias of CO emitters.

1.1 Creating Galaxies

The initial seeds that created the large scale structure of the universe all came from tiny perturbations which are observable today in the cosmic microwave background. These slight differences in density caused dark matter to clump together. These clumps of dark matter pulled in gas, cre-

ating giant clouds. Some of the gas further collapsed to create stars, which in turn formed galaxies.

As a result of this process, galaxies are composed of gas, dust, and stars in various quantities, and so evolve in different ways. Starburst galaxies, for example, are undergoing massive amounts of star formation, and therefore are very bright and use up the gas available to them fairly quickly. On the other hand, main sequence galaxies tend to have much lower star formation rates, and therefore deplete their gas at a much slower rate [3, 4].

These differences in behavior result in varying amounts and types of light being emitted from different types of galaxies. Young stars, for example, tend to emit more of their light in the ultraviolet, and so galaxies with large amounts of ultraviolet light tend to have had large amounts of recent star formation. Gas, on the other hand, tends to absorb the ultraviolet and visible light emitted by stars and re-emits the light at longer wavelengths, such as the infrared. By looking at all the light that a galaxy emits therefore, the properties and makeup of a galaxy can be estimated.

1.2 Observing Galaxies

Parts of a galaxy are easy to observe, and other parts are not. Stars are relatively simple to observe; simply point a telescope like Hubble for long enough at a particular point in the sky and stars become visible. Gas on the other hand, especially the cold gas that collapses to form stars, is much more difficult to detect.

Most of the gas in the universe is made up of hydrogen. Unfortunately for astronomers, molecular hydrogen, H_2 , is only bright enough to observe when it is relatively hot, around 500 Kelvin [1]. As the cold gas that births stars does not usually reach 500 Kelvin, carbon monoxide (CO) is observed instead. CO is the second most common molecule after H_2 , but has the advantages of having bright rotational transitions that can be observed all the way to very high redshifts [1, 2]. Additionally, the amount of H_2 gas present can be inferred from the amount of CO that can be detected by using a conversion factor α_{CO} [1].

These CO transition lines show up in the radio and (sub)mm spectrum, requiring telescopes such as ALMA and the Jansky Very Large Array (VLA) to be used to detect them on Earth [1].

1.3 From Observations to Models

All observations of a galaxy recorded in gamma and X-rays, visible light, infrared, radio and other wavelengths gives us part of the total spectral energy distribution (SED) of that galaxy. The more wavelengths a galaxy is measured in, the better constrained the SED, and the more complete our understanding of its energy distribution. Software, such as MAGPHYS [5, 6], can use these observations to estimate a galaxy's physical parameters. These programs match the observed SED to precomputed models and outputs likelihood estimates for the properties of a given galaxy, such as the star formation rate, mass, dust temperature, and more.

1.4 Galaxies in Groups

The next stage after observing and modeling individual galaxies is to look at galaxies in clusters. By looking at the distribution of galaxies in a given region of space we can determine how densely packed together they are and that in turn, gives us an insight into the amount of dark matter that surrounds them.

Galaxies are not distributed entirely randomly in the universe. On the largest scales, the universe is isotropic and homogeneous, but on smaller scales, galaxies tend to cluster in space. One way to quantify how densely packed a population of galaxies is to compute the so-called two-point correlation function. This allows for the measuring of the mass of the dark matter halos in which these galaxies reside [7]. The more clustered a population of galaxies are, the more massive the halo that they are in.

This report is organized as follows. Chapter 2 focuses on the setup of the survey, the methods used to detect and cross-match lines, and the properties of those matched galaxies. Chapter 3 focuses on the clustering of CO emitters in the survey volume, and compares the clustering of sources in this survey to those of other populations of galaxies. The final chapter, Chapter 4, contains the conclusions and possible future work.

In this report, the Λ CDM cosmology is assumed, with $H_0=70$ km/s/Mpc, $\Omega_m = 0.3$, and $\Omega_\lambda = 0.7$, consistent with the results from the Planck Collaboration [8]. The analysis code used in this report is available here: https://github.com/jacobbieker/Wide_ASPECS.

Chapter 2

Spectral Line Survey

2.1 Previous Work

There have been two main types of surveys for searching for CO emitters in the universe, targeted and blind surveys. In targeted surveys, targets are chosen based on some type of preselection, such as star formation rate, mass, or some other parameter [1, 2], and are looked at specifically to see what CO emissions can be found in that galaxy or galaxies. While these surveys have given useful information on the role gas plays in these galaxies, the preselection process means that there could be a bias in our knowledge of CO. For example, these surveys could miss out on dark, gas-rich galaxies that are hard to detect, giving us an incomplete picture of the variety of galaxies with gas and CO emission in the universe.

Blind surveys are the opposite of targeted surveys. Instead of choosing the targets and looking at them specifically, blind surveys choose an area of the sky and search for any CO emissions within that cosmic volume, allowing for any emissions above the sensitivity limit of the survey to be found. This allows for a sort of census of all the gas within a cosmic volume [1].

Previous blind surveys include the COLDz survey in the GOODS-North region, the PdBI survey, as well as the first two surveys in the ASPECS program, ASPECS Pilot and ASPECS Large Program.

The PdBI survey was a molecular line survey in the Hubble Deep Field North (HDF-N) in 3mm using the IRAM Plateau de Bure Interferometer (PdBI) [9]. This survey was designed to cover all CO transitions detectable above $z > 2$, and well as covering the redshift ranges of $z < 0.45$, and $1 < z < 1.9$. The survey identified 17 line candidates, with most of the candidates falling in intermediate redshifts ($z < 3$), and with 7 of the line

candidates matching to galaxies in their catalog [9].

COLDz, or the CO Luminosity Density at High-z (COLDz) targeted CO(1-0) emissions from galaxies at redshifts between 1.95-2.85 and CO(2-1) emission between $z = 4.91 - 6.70$ using the Very Large Array (VLA)[10]. This survey aimed to perform a similar role as ASPECS, covering a wide area of around 51 arcminute², as well as a roughly 9 arcminute² area much more deeply. This survey blindly selected starburst and massive main sequence galaxies in the GOODS-North and COSMOS fields. COLDz found seven secure CO line detections, and 57 above their S/N threshold, including many that did not have optical or near infrared counterparts, suggesting that those candidates could potentially be from a population of gas-rich, but optically dark galaxies [10].

The ASPECS Pilot and Large Programs both looked at regions in the Hubble Ultra Deep Field. The Pilot program looked incredibly deeply in the 1.2mm and 3mm bands at a small, one arcsecond region of the Hubble eXtremely Deep Field (XDF). The spectral coverage of the Pilot meant that it could detect CO transitions almost continuously from $z = 0$ to $z = 8$, as well as CII emissions from $z = 6$ to $z = 8$ [2]. This allowed for the characterization of CO emitters all the way to a $z = 8$, as well as giving constraints on the knee of the CO luminosity function [2].

The Large Program looked wider, but shallower, covering a roughly five square arcminute area of the Hubble Ultra Deep Field (HUDF) surrounding the ASPECS Pilot region. It was a 150 hour molecular deep field taken at 1.2mm and 3mm [1]. The greater volume probed by the Large Program allowed for constraining the density of gas in the universe, as well as better constraints on the CO luminosity function. The survey blindly revealed the molecular gas content in normal, star-forming main-sequence galaxies [1].

2.2 This Survey

The Wide ASPECS survey builds upon the Pilot and Large Program, going much wider, but also shallower. This means that Wide ASPECS cannot capture as dim CO emitters, but because of the much larger cosmic volume looked at, it can find rarer, but very bright CO emitters that did not happen to fall within the Large Program and Pilot survey bounds.

The data for this survey was observed in ALMA Cycle 5 and was observed in Band 3 (3mm) for 20 hours in 130 pointings and six frequency settings. The survey covered 52.5 arcminutes² of the sky at 20% sensitivity, and 43 arcminutes² at 50% sensitivity. This means Wide ASPECS covers

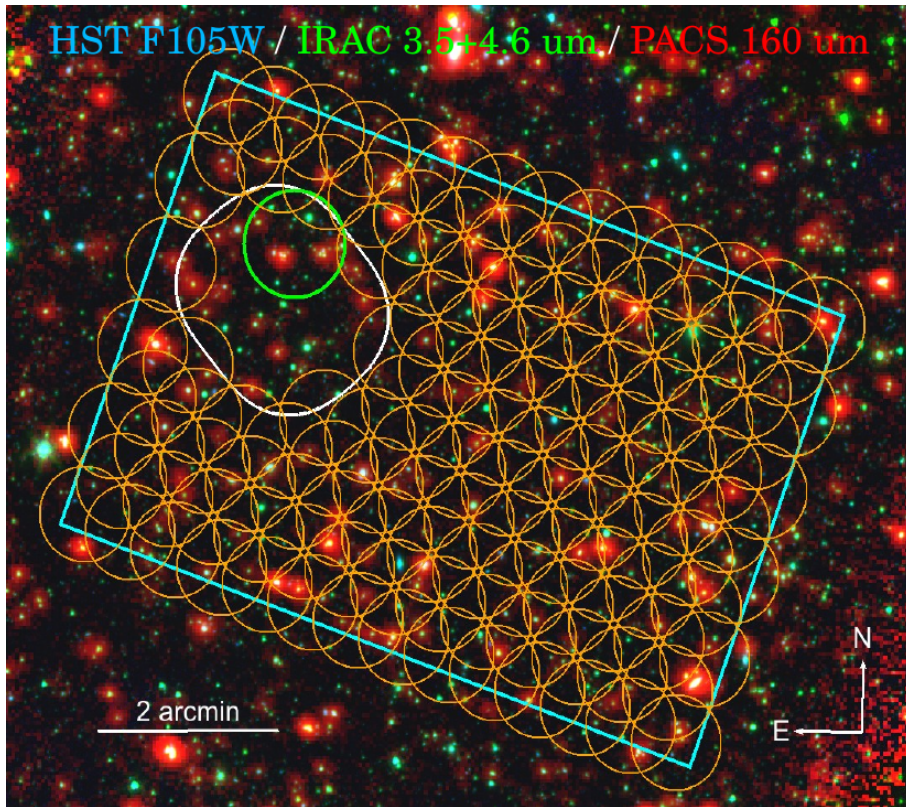


Figure 2.1: Spatial coverage of ASPECS Pilot (Green), Large Program (White), and Wide (Yellow) showing each of the individual pointings. The area covered by the Pilot is 1 arcmin^2 , by the Large Program 5 arcmin^2 , and by Wide ASPECS, 52.5 arcmin^2 . The cyan box is the 50% sensitivity extent of the survey. This region covers the area of the deepest CANDELS observations, where a wealth of ancillary data has been collected in over 30 wavelengths [CITE SURVEY DESCRIPTION].

roughly five times the area of the ASPECS Large Program. This raw data was processed with the CASA ALMA pipeline into six datacubes, one for each frequency setting.

2.2.1 Ancillary Data

In addition to each of those datacubes, there is a lot of ancillary data available as the GOODS-South region is one of the most studied regions of the sky. This data has been collected through combining multiple other catalogs, first described in [2] and expanded with new data in [1], comprising over 30 wavelength bands for over 63000 galaxies in and around the footprint of Wide ASPECS. 26251 galaxies lie within the footprint of Wide

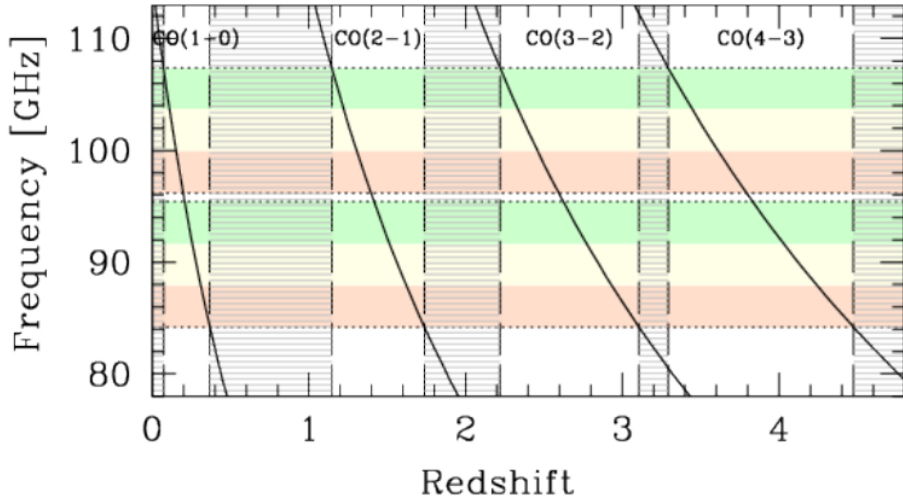


Figure 2.2: Spectral and redshift coverage of Wide ASPECS in relation to the redshift distribution of galaxies within the survey field. Wide ASPECS is designed to detect CO line transitions at $z < 0.4$, $1.1 < z < 1.8$, and $2.2 < z < 4.4$. [CITE SURVEY DESCRIPTION]

Table 2.1: Redshift limits and cosmic volume probed for each CO transition observable by Wide ASPECS.

Transition	z_{low}	z_{high}	Freq. (GHz)	Volume (Mpc^3)
1-0	0.0030	0.3694	115.271	4461
2-1	1.0059	1.7387	230.538	107411
3-2	2.0088	3.1080	345.796	191232
4-3	3.0115	3.3771	461.041	237143

ASPECS, of which 2283 have spectroscopic redshifts, and 23968 have photometric redshifts.

The majority of the ancillary data comes from the Hubble Space Telescope (HST) Cosmic Assembly Near-infrared Deep Extragalactic Legacy Survey (CANDELS)[11, 12]. Most of the photometric data comes from [13], which additionally includes ground-based optical and NIR photometry from [14–20], as well as Spitzer IRAC $3.6\mu\text{m}$, $4.5\mu\text{m}$, $5.8\mu\text{m}$, and $8.0\mu\text{m}$ photometry from [21–23]. There is also data from the Spitzer MIPS $24\mu\text{m}$ photometric information from [24], and ALMA 1.1mm data from [25]. Additional far-infrared data from Herschel PACS at $100\mu\text{m}$ and $160\mu\text{m}$ as obtained from [22]. Spectroscopic redshifts came mostly from the MUSE Hubble Ultra Deep Survey [26, 27], while more spectroscopic information was included from [13, 28–30]. Hubble grism spectroscopy was taken from the 3D-HST survey [31]. All these catalogs were merged into a single catalog through matching sources within 0.5 arcseconds for the photometry, and 1.0 arcseconds for the spectroscopic data. Finally, these matches were then cross-matched with morphological parameters from [32].

2.2.2 SED Fitting

To estimate the properties of the galaxies in the catalog, the SED fitting program MAGPHYS was used [5, 6]. MAGPHYS computes a marginalized likelihood distribution for each of the different physical parameters of the observed galaxy through comparing the observed SED with the pre-computed models. It also outputs the best-fit total SED for a given galaxy. In this report, the MAGPHYS high-z extension was used [6].

An example output from MAGPHYS is shown in Fig. 2.3, showing the model, the likelihood values for various physical properties of the galaxy, and the data points used to compute the SED in red. The distribution of the stellar mass, and star formation rates of all the galaxies fitted with MAGPHYS are shown in Fig. 2.5. Galaxies whose computed star formation rate was at or below a $\log_{10}(SFR) = -1.99$ were removed from the rest of the analysis, as this seemed to indicate a very poor MAGPHYS fit. That left a total of around 55000 galaxies in the sample, of which 22073 were in the Wide ASPECS footprint.

2.3 Method

As an overview, the method for finding lines, computing the fidelity, cross-matching, and determining matches is the same process as used in the

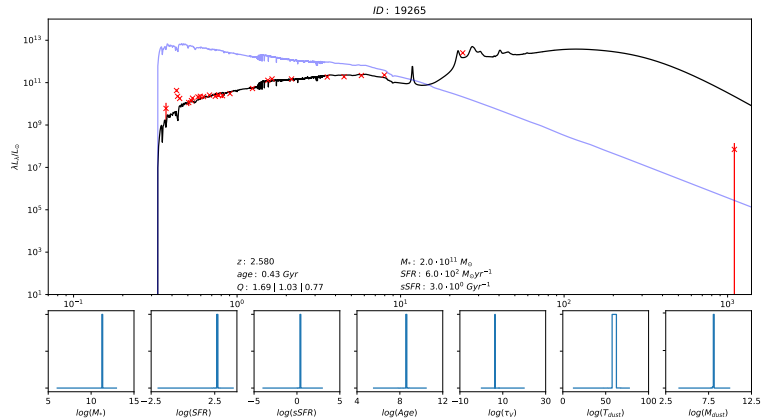


Figure 2.3: Example MAGPHYS output, from the most massive matched galaxy, ID.9 in Table 2.4.1. The blue line is the spectrum of the galaxy without attenuation. The black line is the model used by MAGPHYS. The red dots are the data points. The bottom row of graphs show the probability distribution for various physical properties.

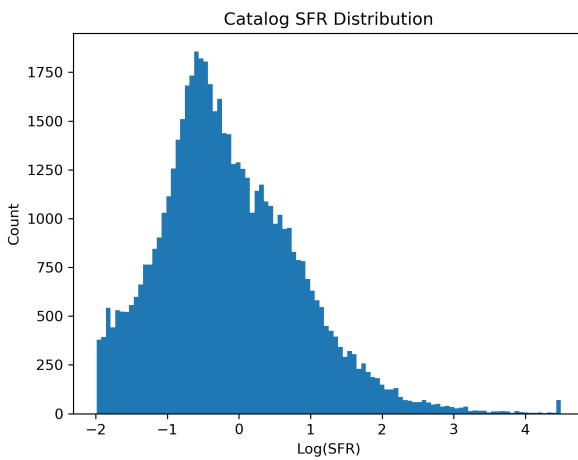


Figure 2.4: Distribution of star formation rate for all galaxies in the catalog. The cutoff at -1.99 is from the quality cut to remove galaxies that had very poor MAGPHYS fits.

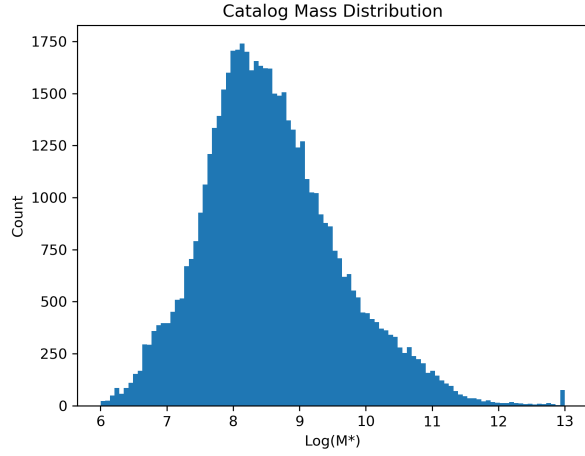


Figure 2.5: Distribution of mass for all galaxies in the catalog. These galaxies have undergone the same quality cut as for the star formation rate plot.

other ASPECS surveys [1, 2, 33].

2.3.1 Line Search and Fidelity

To find possible CO emitters, a search for CO lines was done with the Find-Clump algorithm first described in [2]. This code searches along the spectral axis with different kernel widths in order to maximize the sensitivity to signal associated with line candidates of different intrinsic widths. The widths range from 3 spectral channels up to 19 channels, with each channel being 7.813 MHz wide. The data cubes are searched for lines at any spatial position and spectral coordinate, without any prior based on data from other wavelengths. This is done to minimize any bias in the selection. FindClump returns a list of potential line candidates that then have duplicates removed, which is done by grouping line candidates based on their spatial and spectral position in the cube from each group, only storing the candidate with the highest S/N. This results in 11941 candidates at S/N>5.0, 1096 at S/N>5.5, 78 at S/N>6.0, and 6 at S/N>6.5.

To get a sense of how many of these line candidates are false positives, the fidelity of the lines are then computed. To obtain the fidelity, a line search on the negative data cubes is performed. The negative cubes are obtained by multiplying all the values in each data cube by -1, and rerunning the line search. This catalog of negative lines is then used to compute the fidelity. The fidelity of a line at a given S/N is defined as

$$fidelity(S/N) = 1 - \frac{N_{neg}(S/N)}{N_{pos}(S/N)}$$

where $N_{pos}(S/N)$ and $N_{neg}(S/N)$ are the number of positive and negative line candidates detected at that S/N and for a given line width[33].

The fidelity of the different line widths are shown in Fig. 2.6. As can be seen, the fidelity of the lines is generally higher for wider line widths as more independent resolution elements are included [1]. For this report, there were 16 lines at a fidelity >0.8 , 20 at >0.7 , 35 at >0.6 , 52 at >0.5 , and 69 at >0.4 . The fidelity cut used for the rest of this analysis is set at 0.6, where every given line has a 60% chance of being a real line, and leaving us with 35 line candidates. A breakdown of the number of line candidates as a function of the channel width is shown in Table 2.2.

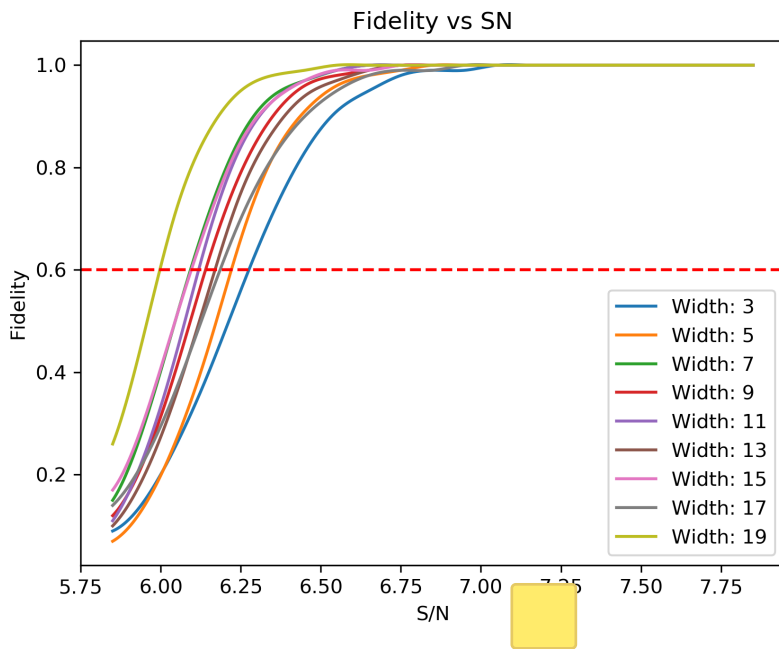


Figure 2.6: Fidelity vs S/N for the different widths used by FindClump. The red dotted line shows the fidelity = 0.6 cutoff used for the analysis in this report. There are a total of 35 line candidates above that cutoff.

2.3.2 Cross-matching and Redshift Determination

Once the lines have been found, and the fidelity computed, the next step is to cross-match the CO lines to already known galaxies within the Wide AS-

Table 2.2: Number of sources, and S/N cutoffs, per channel width for the adopted fidelity cut of > 0.6 .

Channels	S/N	N. Sources	
3	6.28	3	
5	6.22	4	
7	6.09	8	
9	6.14	2	
11	6.12	6	
13	6.17	4	
15	6.10	3	
17	6.19	3	
19	6.00	2	

PECS footprint. To do this, the spatial location of the line candidates were matched to galaxies that were within one arcsecond of the line candidate's location. Then, assuming that the CO line is from that matched galaxy, the CO transition was calculated. The match was only kept if the offset between the CO line's redshift and the galaxy's redshift, δz , was ($|\delta z| < 0.01$) for galaxies with spectroscopic redshifts, or ($|\delta z| < 0.3$) for ones with photometric redshifts. The differences in $|\delta z|$ thresholds is because spectroscopic redshifts are much more reliable and precise than photometric redshifts.

If a line matches to more than a single galaxy, then the following steps are performed to differentiate which galaxy the line should be matched to. The first step is to calculate the CO transition for the line assuming the line is matched to each of the galaxies. Once that is determined, the difference in redshift between the CO redshift and the galaxy's redshift is calculated. The matched galaxy that gives the smallest $|\delta z|$, and whose redshift falls within the limits of Wide ASPECS, is then saved as the matched galaxy for that line candidate.

If there is not a match to a galaxy in the catalog, or if the galaxy's redshift is incompatible with the CO line identification, then the line identification is performed by a bootstrap method, where the probability of a line candidate being one of CO(1-0), CO(2-1), CO(3-2), or CO(4-3) is proportional to the volume of the universe sampled in each of those transitions [1, 2].

2.4 Results

The mass versus star formation rate is shown for the general galactic population and the ASPECS sources in Fig. 2.7. For comparison, the Schreiber et al. 2015 [34] and Whitaker et al. 2014 [24] main sequence fits are plotted as well. As can be seen, two of the matched galaxies are above the main sequence and are massive, star-forming galaxies that are the expected type of galaxies for this survey to match to. The other galaxy is much less massive than expected.

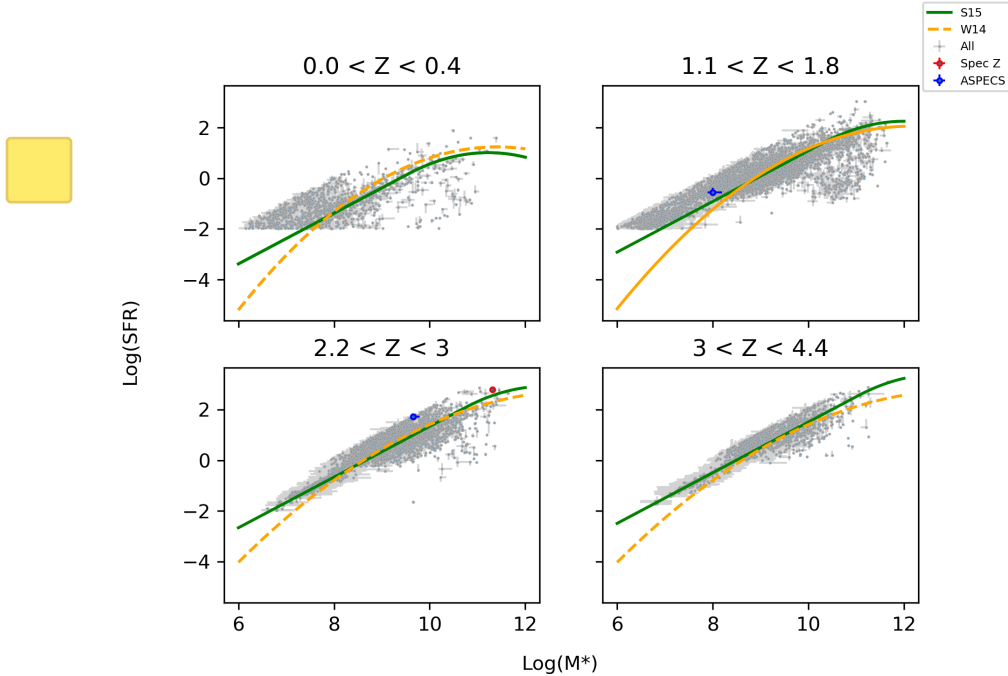


Figure 2.7: Mass vs Star Formation Rate for the matched galaxies. Red points are matched galaxies with spectroscopic redshifts, while blue points are matched galaxies with photometric redshifts. Grey points are all the galaxies in the catalog. The green lines are the galaxy main sequence fits from [34]. The yellow line is from [24]'s galactic main sequence fit, where the solid line means it is computed within the range mentioned in the paper, while dotted means that the values are extrapolated from the paper to higher, or lower, redshifts. Two of the three matches are on the upper edge of the main sequence, while the third match has a much lower mass and star formation rate than expected for this survey. Error bars are the 16/84th percentile outputs from MAGPHYS.

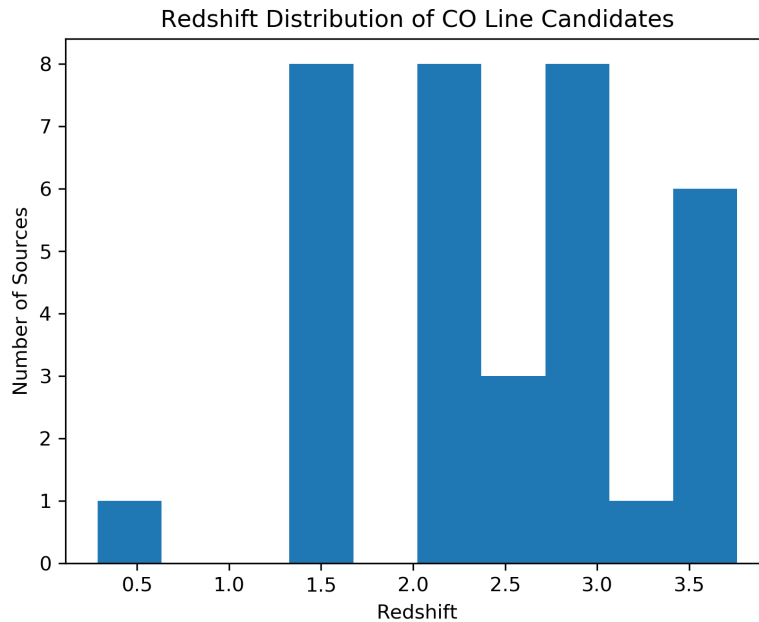


Figure 2.8: Redshift distribution for the CO redshifts.

2.4.1 Catalog

The final catalog of CO line emitters is shown in Table 2.4.1. 3 lines match to galaxies in the catalog. Of those three matches, only ID.1's match has a spectroscopic redshift. The redshift distribution of the whole catalog is shown in Fig. 2.8, and some of the physical properties of the three matched lines is shown in Table. 2.4.

In addition, the line candidates are shown overlaid over other wavelengths in the Appendix ??.

2.5 Discussion

There are significantly less matches than was expected. Only 9% percent of the lines match to galaxies. Of those that do, only two matched to the kind of galaxies that were expected, which are the most massive, most star forming galaxies in the field.

Possible explanations include issues with MAGPHYS' fitting of the galaxies in the catalog, as many of the galaxies seem poorly constrained.

Table 2.3: RA and DEC are in the J2000 system. v_{CO} is the observed frequency of the source in GHz. CO Tran. is the estimated CO transition. If available, δz is the redshift difference between the source and the matched galaxy. S/N is the signal-to-noise of the source. Match tells whether there is a match to a galaxy in the catalog. Only ID.1 has a matched galaxy with a spectroscopic redshift.

ID	RA	DEC	v_{CO}	CO Tran.	z_{CO}	δz	S/N	Match?
ID.1	53.14886	-27.82118	96.701	3-2	2.576	0.006	7.31	Y
ID.2	53.19145	-27.76985	91.657	2-1	1.515	–	6.82	N
ID.3	53.14138	-27.84409	96.834	4-3	3.761	–	6.72	N
ID.4	53.19242	-27.78342	106.72	3-2	2.24	–	6.63	N
ID.5	53.16066	-27.76629	86.677	2-1	1.66	-0.237	6.6	Y
ID.6	53.16003	-27.76258	103.36	3-2	2.346	–	6.6	N
ID.7	53.13447	-27.74976	102.719	3-2	2.366	–	6.49	N
ID.8	53.11066	-27.82727	85.654	3-2	3.037	–	6.45	N
ID.9	53.11881	-27.78291	104.501	3-2	2.309	0.081	6.43	Y
ID.10	53.13921	-27.75352	86.67	3-2	2.99	–	6.43	N
ID.11	53.07696	-27.8251	90.891	2-1	1.536	–	6.42	N
ID.12	53.12766	-27.76666	99.553	4-3	3.631	–	6.42	N
ID.13	53.07796	-27.80182	98.725	4-3	3.67	–	6.36	N
ID.14	53.13923	-27.78228	94.407	2-1	1.442	–	6.35	N
ID.15	53.04266	-27.79322	103.173	3-2	2.352	–	6.3	N
ID.16	53.116	-27.84624	97.569	4-3	3.725	–	6.29	N
ID.17	53.09146	-27.8497	106.235	3-2	2.255	–	6.27	N
ID.18	53.18748	-27.81369	89.704	1-0	0.285	–	6.27	N
ID.19	53.11238	-27.75628	88.735	3-2	2.897	–	6.26	N
ID.20	53.12915	-27.79241	91.54	2-1	1.518	–	6.22	N
ID.21	53.1179	-27.8184	92.876	2-1	1.482	–	6.21	N
ID.22	53.06549	-27.84266	104.094	3-2	2.322	–	6.21	N
ID.23	53.1612	-27.76049	94.618	2-1	1.437	–	6.19	N
ID.24	53.11182	-27.82032	99.522	4-3	3.633	–	6.19	N
ID.25	53.07121	-27.82724	88.954	3-2	2.887	–	6.17	N
ID.26	53.19977	-27.8282	100.055	3-2	2.456	–	6.16	N
ID.27	53.06316	-27.82356	84.623	3-2	3.086	–	6.15	N
ID.28	53.09788	-27.76003	90.618	3-2	2.816	–	6.13	N
ID.29	53.16282	-27.84445	90.571	3-2	2.818	–	6.12	N
ID.30	53.09665	-27.81229	95.259	2-1	1.42	–	6.12	N
ID.31	53.13844	-27.80491	102.376	3-2	2.378	–	6.12	N
ID.32	53.16516	-27.82257	104.931	3-2	2.295	–	6.11	N
ID.33	53.19483	-27.81481	98.873	4-3	3.663	–	6.1	N
ID.34	53.08948	-27.78102	86.068	3-2	3.018	–	6.1	N
ID.35	53.14828	-27.84444	87.302	3-2	2.961	–	6.1	N

Table 2.4: This shows some of the physical parameters for the 3 matched line candidates. Sep is the separation in arcseconds between the CO line and the galaxy. $z_{catalog}$ is the master catalog's redshift for the galaxy.

ID	Trans.	z_{CO}	$z_{catalog}$	δz	Spec	S/N	Sep	Log(SFR)	Log(M^*)
ID.1	3-2	2.576	2.582	0.006	Y	7.31	0.2824	$2.782^{+0.005}_{-0.005}$	$11.31^{+0.0}_{-0.0}$
ID.5	2-1	1.66	1.423	-0.237	N	6.6	0.9723	$-0.453^{+0.255}_{-0.255}$	$8.017^{+0.175}_{-0.175}$
ID.9	3-2	2.309	2.39	0.081	N	6.43	0.4861	$1.307^{+0.0}_{-0.0}$	$9.757^{+0.0}_{-0.0}$

Chapter 3

Clustering

Wide ASPECS' well-defined, large cosmic volume allows for some of the first direct constraints on the clustering bias of CO emitters. This clustering bias can be then used to constrain the typical halo mass in which they reside [35].

3.1 Previous Work

Previous work on clustering has been looked at different populations of galaxies. [7] looked at the clustering of quasars and obscured quasars. [35] looks at the clustering in SMGs and compares their clustering to clustering found for other sets of astronomical objects, as can be seen in Fig. 3.1. [7] found, in the Boötes field, an r_0 for unobscured quasars to be 5.6 ± 0.8 , and for obscured quasars 6.0 ± 1.0 . In [35], SMGs in the Extended Chandra Deep Field South were found to have a r_0 of $7.7^{+1.8}_{-2.3}$.

3.2 Method

3.2.1 Angular Correlation Function

The clustering is computed through a two point correlation function. The first step is to calculate the angular correlation function $\omega(\theta)$. Once $\omega(\theta)$ is computed, the second step is to obtain the two-point correlation function parameters of r_0 and γ .

The two-point correlation function, $\xi(r)$ is the probability of finding a galaxy at a separation r from another randomly chosen galaxy in a

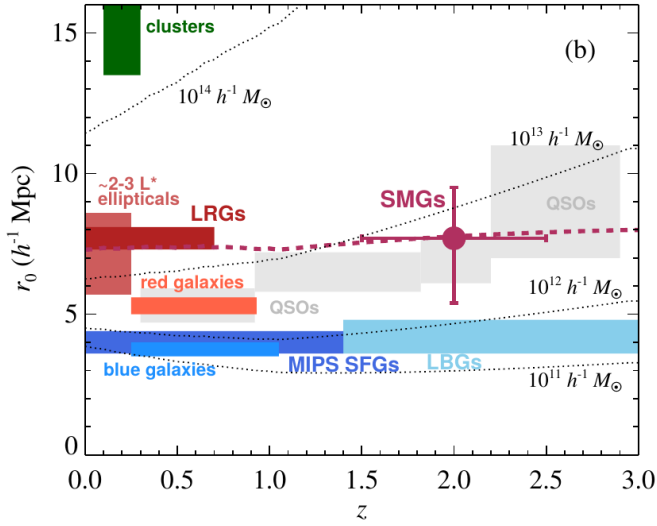


Figure 3.1: r_0 values for a variety of celestial objects as a function of redshift. The grey dotted lines show the evolution of r_0 for dark matter haloes of different masses. Figure adapted from [35].

volume dV above Poisson, such that

$$dP = n(1 + \xi(r))dV$$

, where n is the mean space density of the galaxies in the sample[7].

To calculate the angular correlation function, the estimator from [36] is used, where

$$\omega(\theta) = \frac{1}{RR}(DD - 2DR + RR)$$

, where DD , DR , and RR are the number of data-data, data-random, and random-random galaxy pairs at a separation θ , where each of the three collections is normalized to sum to 1 [7].

Once the angular correlation function is found, a power-law model is fitted following

$$\omega(\theta) = A\theta^{-\beta}$$

where $\beta = 0.8$, a value used for many other galaxy angular correlations [7].

3.2.2 Obtaining r_0 and γ

Two equations are used to convert the A and β to real-space r_0 and γ ,

$$\gamma = \beta + 1$$

and

$$A = H_\gamma \frac{\int_0^{\inf} (dN_1/dz)(dN_2/dz) E_z \chi^{1-\gamma} dz}{[\int_0^{\inf} (dN_1/dz) dz][\int_0^{\inf} (dN_2/dz) dz]} r_0^\gamma$$

where $H_\gamma = \Gamma(0.5)\Gamma(0.5[\gamma - 1])\Gamma(0.5\gamma)$, with Γ being the gamma function, χ the radial comoving distance, $dN_{1,2}/dz$ are the redshift distributions of the samples, where in the case of autocorrelation are equal to each other, and $E_z = H_z/c = dz/d\chi$ [7]. The Hubble parameter H_z can be found from

$$H_z^2 = H_0^2 [\Omega_m (1+z)^3 + \Omega_\lambda]$$

[7].

For this analysis, all CO line candidates above the 0.6 fidelity threshold were used, resulting in 35 sources, shown in Fig. 3.2. Two catalogs of random points were created, of 20000 points each, and their angular correlation computed to show that it is consistent with zero, shown in Fig. 3.3. As a comparison, the two point correlation function was also computed for other fidelity cuts. The redshift distribution was taken from the CO redshifts of the lines, and the calculations were calculated over the range $z = 1.5$ to 3.5 , as this is the range where most of the CO candidates seem to lie. To calculate $dN_{1,2}/dz$, the redshift distribution of the CO lines was fitted with a Gaussian, and the integral was taken over the Gaussian fit. The angular correlation function was computed over the range of 8.39 to 582.10 arcseconds, using logarithmically spaced bins.

3.3 Results

As can be seen in Fig. 3.4, as the fidelity increases, A increases as well. When converted to r_0 , the fidelity cuts result in r_0 values of $7.89^{+5.83}_{-7.89}$ for fidelity > 0.7 , $7.22^{+0.83}_{-0.9}$ for fidelity > 0.6 , $0.0^{+4.03}_{-0.0}$ for fidelity > 0.5 , and $r_0 = 0.0^{+0.0}_{-0.0}$ for fidelity > 0.4 , as the A value is always negative.

Besides the different fidelity cuts, different binnings also are included to study their effects on the final r_0 results. The results seem to be very dependent on the binning. While the values for the only positively fitted bins does not change dramatically as the binning changes, the number of bins does make a large difference in the final A , and therefore r_0 values, as can be seen in Figures 3.6 and 3.7 in comparison to Fig. 3.5.

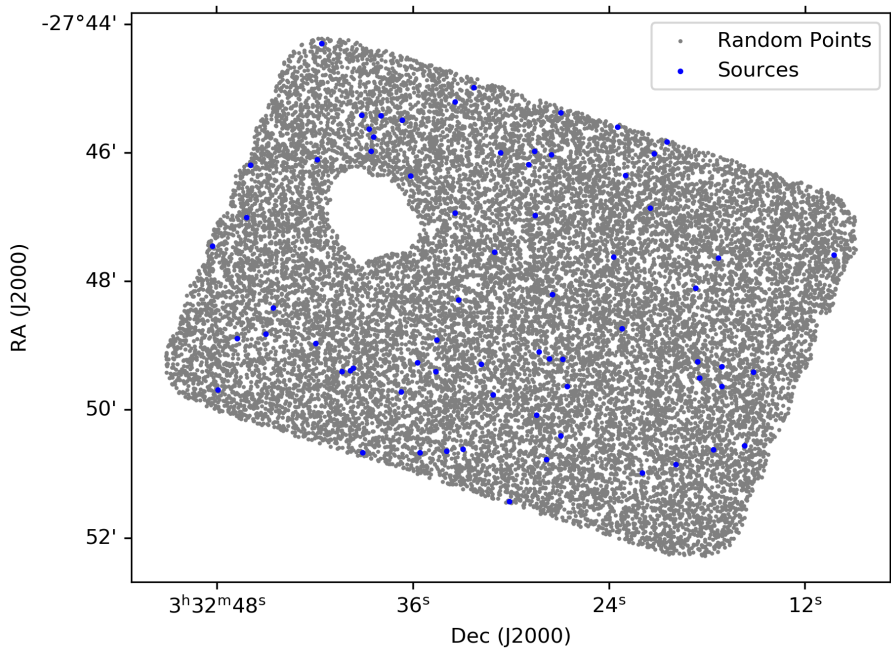


Figure 3.2: Random points and sources from the > 0.6 fidelity cut. The random points are distributed uniformly throughout the Wide ASPECS footprint.

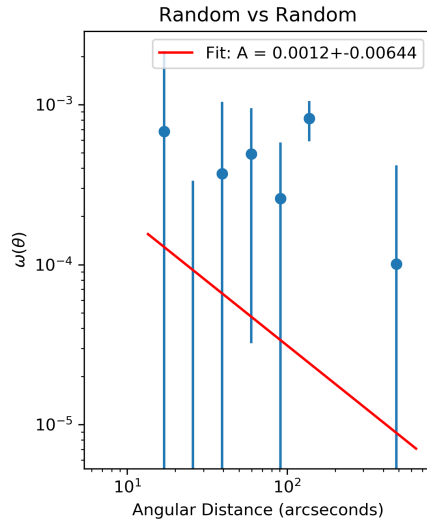


Figure 3.3: Angular correlation two sets of random points used in this analysis, showing that the angular correlation is consistent with zero, as would be expected for uniformly distributed points.

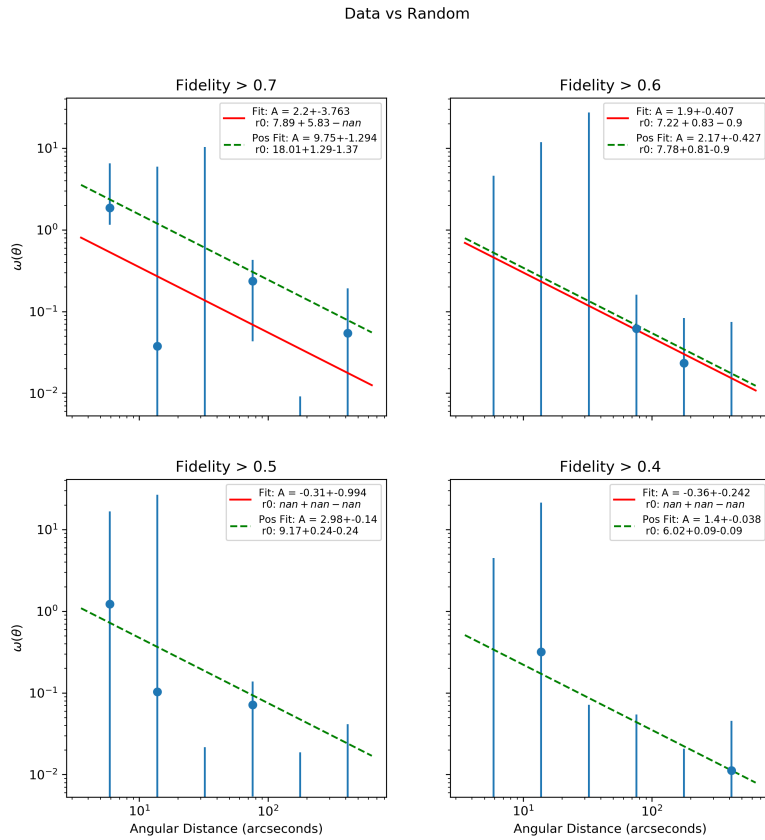


Figure 3.4: Angular correlation function for various fidelity cuts. The bins increase logarithmically from 8.39 arcsecs to 582.10 arcseconds. The red lines are from fitting $\omega(\theta) = A\theta^{-0.8}$ to all of the bins. The green dashed line is from fitting that same equation only to bins that had a positive value. As the fidelity goes up, the A value increases as well, indicating stronger clustering. The few line candidates means that the results are quite noisy, and are sensitive to the bins chosen.

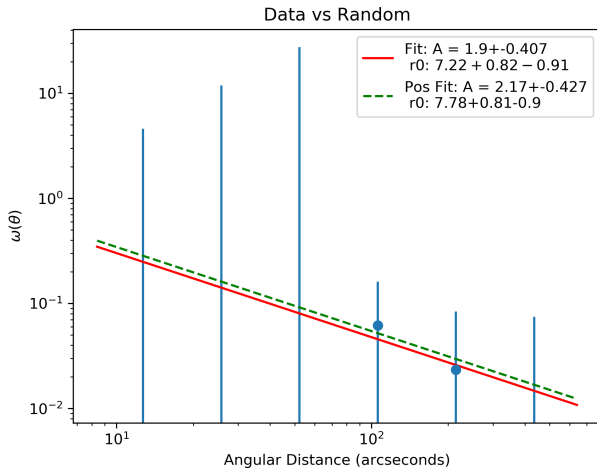


Figure 3.5: Angular correlation function for 6 bins for the chosen fidelity cut of 0.6. Red is the fit $\omega(\theta) = A\theta^{-0.8}$ to all the bins, while the green line is the fit to only the positive bins. This is the final binning used for the analysis.

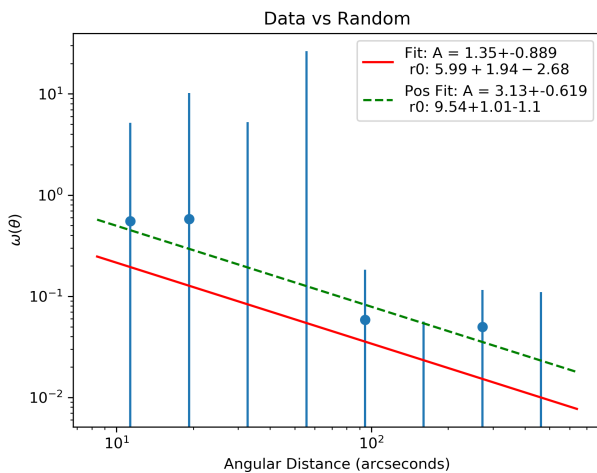


Figure 3.6: Angular correlation function for 8 bins for fidelity > 0.6 . In this case, an increase in the number of bins decreases the r_0 value, although it is still consistent with the original r_0 value.

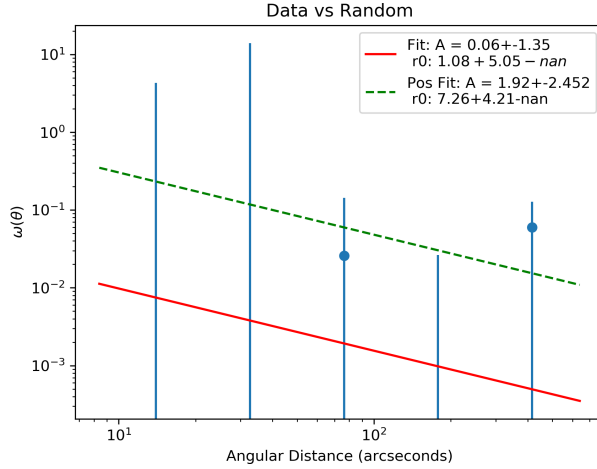


Figure 3.7: Angular correlation function for 5 bins for fidelity > 0.6 . In this case, decreasing the number of bins also decreases the r_0 value, which are not consistent with the r_0 found originally.

3.4 Discussion

The clustering results do show that there is a larger r_0 as the fidelity cut becomes higher, suggesting that there are real sources in the sample. On the other hand, the clustering measurement is still very noisy and future work will be required to get a better final clustering measurement. The current measurement for r_0 seems to depend greatly on the number of bins chosen.

In comparison to previous results, the r_0 of the CO emitters here are quite similar to the values for the SMGs found in [35].

Chapter **4**

Conclusion

[INCLUDE CONCLUSION]

4.1 Future Work

While these results are interesting, they are quite tentative. The clustering results could be improved through performing the cross-correlation between the CO line candidates and the galaxy catalog [7, 35, 37].

Additional work could be done to verify the CO lines matched to galaxies, and investigate the reasons as to why the matched galaxies are much less massive and star forming than expected.

Bibliography

- [1] Roberto Decarli, Fabian Walter, Jorge Gómez-López, Manuel Aravena, Leindert Boogaard, Chris Carilli, Pierre Cox, Emanuele Daddi, Gergö Popping, Dominik Riechers, et al. The alma spectroscopic survey in the hudf: Co luminosity functions and the molecular gas content of galaxies through cosmic history. *arXiv preprint arXiv:1903.09164*, 2019.
- [2] Fabian Walter, Roberto Decarli, Manuel Aravena, Chris Carilli, Rychard Bouwens, Elisabete Da Cunha, Emanuele Daddi, Robert J Ivison, Dominik Riechers, Ian Smail, et al. Alma spectroscopic survey in the hubble ultra deep field: survey description. *The Astrophysical Journal*, 833(1):67, 2016.
- [3] N Scoville, N Lee, P Vanden Bout, T Diaz-Santos, D Sanders, B Darvish, A Bongiorno, CM Casey, L Murchikova, J Koda, et al. Evolution of interstellar medium, star formation, and accretion at high redshift. *The Astrophysical Journal*, 837(2):150, 2017.
- [4] John D Silverman, Emanuele Daddi, Giulia Rodighiero, Wiphu Ru-jopakarn, Mark Sargent, Alvio Renzini, Daizhong Liu, Chiara Feruglio, Daichi Kashino, David Sanders, et al. A higher efficiency of converting gas to stars pushes galaxies at $z \geq 1.6$ well above the star-forming main sequence. *The Astrophysical Journal Letters*, 812(2):L23, 2015.
- [5] Elisabete Da Cunha, Stéphane Charlot, and David Elbaz. A simple model to interpret the ultraviolet, optical and infrared emission from galaxies. *Monthly Notices of the Royal Astronomical Society*, 388(4):1595–1617, 2008.

- [6] Elisabete da Cunha, Fabian Walter, IR Smail, AM Swinbank, JM Simpson, Roberto Decarli, JA Hodge, Axel Weiss, PP van der Werf, Frank Bertoldi, et al. An alma survey of sub-millimeter galaxies in the extended chandra deep field south: physical properties derived from ultraviolet-to-radio modeling. *The Astrophysical Journal*, 806(1):110, 2015.
- [7] Ryan C Hickox, Adam D Myers, Mark Brodwin, David M Alexander, William R Forman, Christine Jones, Stephen S Murray, Michael JI Brown, Richard J Cool, Christopher S Kochanek, et al. Clustering of obscured and unobscured quasars in the boötes field: Placing rapidly growing black holes in the cosmic web. *The Astrophysical Journal*, 731(2):117, 2011.
- [8] Peter AR Ade, N Aghanim, M Arnaud, M Ashdown, J Aumont, C Baccigalupi, AJ Banday, RB Barreiro, JG Bartlett, N Bartolo, et al. Planck 2015 results-xiii. cosmological parameters. *Astronomy & Astrophysics*, 594:A13, 2016.
- [9] R Decarli, F Walter, C Carilli, D Riechers, P Cox, R Neri, M Aravena, E Bell, F Bertoldi, D Colombo, et al. A molecular line scan in the hubble deep field north. *The Astrophysical Journal*, 782(2):78, 2014.
- [10] Riccardo Pavesi, Chelsea E Sharon, Dominik A Riechers, Jacqueline A Hodge, Roberto Decarli, Fabian Walter, Chris L Carilli, Emanuele Daddi, Ian Smail, Mark Dickinson, et al. The co luminosity density at high-z (coldz) survey: A sensitive, large-area blind search for low-j co emission from cold gas in the early universe with the karl g. jansky very large array. *The Astrophysical Journal*, 864(1):49, 2018.
- [11] Norman A Grogin, Dale D Kocevski, SM Faber, Henry C Ferguson, Anton M Koekemoer, Adam G Riess, Viviana Acquaviva, David M Alexander, Omar Almaini, Matthew LN Ashby, et al. Candels: the cosmic assembly near-infrared deep extragalactic legacy survey. *The Astrophysical Journal Supplement Series*, 197(2):35, 2011.
- [12] Anton M. Koekemoer, S. M. Faber, Henry C. Ferguson, Norman A. Grogin, Dale D. Kocevski, David C. Koo, Kamson Lai, Jennifer M. Lotz, Ray A. Lucas, Elizabeth J. McGrath, Sara Ogaz, Abhijith Rajan, Adam G. Riess, Steve A. Rodney, Louis Strolger, Stefano Casertano, Marco Castellano, Tomas Dahlen, Mark Dickinson, Timothy Dolch, Adriano Fontana, Mauro Giavalisco, Andrea Grazian, Yicheng

Guo, Nimish P. Hathi, Kuang-Han Huang, Arjen van der Wel, Hao-Jing Yan, Viviana Acquaviva, David M. Alexander, Omar Almaini, Matthew L. N. Ashby, Marco Barden, Eric F. Bell, Frédéric Bournaud, Thomas M. Brown, Karina I. Caputi, Paolo Cassata, Peter J. Challis, Ranga-Ram Chary, Edmond Cheung, Michele Cirasuolo, Christopher J. Conselice, Asantha Roshan Cooray, Darren J. Croton, Emanuele Daddi, Romeel Davé, Duilia F. de Mello, Loic de Ravel, Avishai Dekel, Jennifer L. Donley, James S. Dunlop, Aaron A. Dutton, David Elbaz, Giovanni G. Fazio, Alexei V. Filippenko, Steven L. Finkelstein, Chris Frazer, Jonathan P. Gardner, Peter M. Garnavich, Eric Gawiser, Ruth Gruetzbauch, Will G. Hartley, Boris HÄussler, Jessica Herrington, Philip F. Hopkins, Jia-Sheng Huang, Saurabh W. Jha, Andrew Johnson, Jeyhan S. Kartaltepe, Ali A. Khstov, Robert P. Kirshner, Caterina Lani, Kyoung-Soo Lee, Weidong Li, Piero Madau, Patrick J. McCarthy, Daniel H. McIntosh, Ross J. McLure, Conor McPartland, Bahram Mobasher, Heidi Moreira, Alice Mortlock, Leonidas A. Moustakas, Mark Mozena, Kirpal Nandra, Jeffrey A. Newman, Jennifer L. Nielsen, Sami Niemi, Kai G. Noeske, Casey J. Papovich, Laura Pentericci, Alexandra Pope, Joel R. Primack, Swara Ravindranath, Naveen A. Reddy, Alvio Renzini, Hans-Walter Rix, Aday R. Robaina, David J. Rosario, Piero Rosati, Sara Salimbeni, Claudia Scarlata, Brian Siana, Luc Simard, Joseph Smidt, Diana Snyder, Rachel S. Somerville, Hyron Spinrad, Amber N. Straughn, Olivia Telford, Harry I. Teplitz, Jonathan R. Trump, Carlos Vargas, Carolin Villforth, Cory R. Wagner, Pat Wand, Risa H. Wechsler, Benjamin J. Weiner, Tommy Wiklind, Vivienne Wild, Grant Wilson, Stijn Wuyts, and Min S. Yun. CANDELS: THE COSMIC ASSEMBLY NEAR-INFRARED DEEP EXTRAGALACTIC LEGACY SURVEY—THEHUBBLE SPACE TELESCOPEOBSERVATIONS, IMAGING DATA PRODUCTS, AND MOSAICS. *The Astrophysical Journal Supplement Series*, 197(2):36, dec 2011.

- [13] Rosalind E Skelton, Katherine E Whitaker, Ivelina G Momcheva, Gabriel B Brammer, Pieter G van Dokkum, Ivo Labbe, Marijn Franx, Arjen van der Wel, Rachel Bezanson, Elisabete Da Cunha, et al. 3d-hst wfc3-selected photometric catalogs in the five candels/3d-hst fields: photometry, photometric redshifts, and stellar masses. *The Astrophysical Journal Supplement Series*, 214(2):24, 2014.
- [14] M Nonino, M Dickinson, Piero Rosati, A Grazian, N Reddy, S Cristiani, M Giavalisco, H Kuntschner, E Vanzella, E Daddi, et al. Deep

- u band and r imaging of goods-south: Observations, data reduction and first results. *The Astrophysical Journal Supplement Series*, 183(2):244, 2009.
- [15] Hendrik Hildebrandt, T Erben, JP Dietrich, O Cordes, L Haberzettl, M Hetterscheidt, M Schirmer, O Schmithuesen, P Schneider, P Simon, et al. Gabods: The garching-bonn deep survey-v. data release of the eso deep-public-survey. *Astronomy & Astrophysics*, 452(3):1121–1128, 2006.
- [16] Thomas Erben, M Schirmer, JP Dietrich, O Cordes, L Haberzettl, M Hetterscheidt, H Hildebrandt, O Schmithuesen, P Schneider, P Simon, et al. Gabods: The garching-bonn deep survey: Iv. methods for the image reduction of multi-chip cameras demonstrated on data from the esowide-field imager. *Astronomische Nachrichten: Astronomical Notes*, 326(6):432–464, 2005.
- [17] J Retzlaff, Piero Rosati, M Dickinson, B Vandame, C Rit , M Nonino, and C Cesarsky. The great observatories origins deep survey-vlt/isaac near-infrared imaging of the goods-south field. *Astronomy & Astrophysics*, 511:A50, 2010.
- [18] Bau-Ching Hsieh, Wei-Hao Wang, Haojing Yan, Lihwai Lin, Hiroshi Karoji, Jeremy Lim, Paul T. P. Ho, and Chao-Wei Tsai. THE TAIWAN ECDFS NEAR-INFRARED SURVEY: VERY BRIGHT END OF THE LUMINOSITY FUNCTION AT $z \approx 7$. *The Astrophysical Journal*, 749(1):88, mar 2012.
- [19] S. Wuyts, I. Labb , N. M. F rster Schreiber, M. Franx, G. Rudnick, G. B. Brammer, and P. G. van Dokkum. FIREWORKS U₃₈-to-24 μ m Photometry of the GOODS Chandra Deep Field-South: Multiwavelength Catalog and Total Infrared Properties of Distant K_s-selected Galaxies. , 682:985–1003, August 2008.
- [20] Carolin N Cardamone, Pieter G Van Dokkum, C Megan Urry, Yoshi Taniguchi, Eric Gawiser, Gabriel Brammer, Edward Taylor, Maaike Damen, Ezequiel Treister, Bethany E Cobb, et al. The multiwavelength survey by yale-chile (musyc): Deep medium-band optical imaging and high-quality 32-band photometric redshifts in the ecdfs. *The Astrophysical Journal Supplement Series*, 189(2):270, 2010.
- [21] Mark Dickinson, Casey Papovich, Henry C Ferguson, and Tamas Budavari. The evolution of the global stellar mass density at 0 $\leq z \leq$ 3. *The Astrophysical Journal*, 587(1):25, 2003.

- [22] D Elbaz, M Dickinson, HS Hwang, T Díaz-Santos, G Magdis, B Magnelli, D Le Borgne, F Galliano, M Pannella, P Chanial, et al. Goods-herschel: an infrared main sequence for star-forming galaxies. *Astronomy & Astrophysics*, 533:A119, 2011.
- [23] M. L. N. Ashby, S. P. Willner, G. G. Fazio, J.-S. Huang, R. Arendt, P. Barmby, G. Barro, E. F. Bell, R. Bouwens, A. Cattaneo, D. Croton, R. Davé, J. S. Dunlop, E. Egami, S. Faber, K. Finlator, N. A. Grogin, P. Guhathakurta, L. Hernquist, J. L. Hora, G. Illingworth, A. Kashlinsky, A. M. Koekemoer, D. C. Koo, I. Labb  , Y. Li, L. Lin, H. Moseley, K. Nandra, J. Newman, K. Noeske, M. Ouchi, M. Peth, D. Rigopoulou, B. Robertson, V. Sarajedini, L. Simard, H. A. Smith, Z. Wang, R. Wechsler, B. Weiner, G. Wilson, S. Wuyts, T. Yamada, and H. Yan. SEDS: The Spitzer Extended Deep Survey. Survey Design, Photometry, and Deep IRAC Source Counts. , 769:80, May 2013.
- [24] Katherine E. Whitaker, Marijn Franx, Joel Leja, Pieter G. van Dokkum, Alaina Henry, Rosalind E. Skelton, Mattia Fumagalli, Ivelina G. Momcheva, Gabriel B. Brammer, Ivo Labb  , Erica J. Nelson, and Jane R. Rigby. CONSTRAINING THE LOW-MASS SLOPE OF THE STAR FORMATION SEQUENCE AT 0.5 \leq z \leq 2.5. *The Astrophysical Journal*, 795(2):104, oct 2014.
- [25] M Franco, D Elbaz, M B  thermin, B Magnelli, C Schreiber, L Ciesla, M Dickinson, N Nagar, J Silverman, E Daddi, et al. Goods-alma: 1.1 mm galaxy survey-i. source catalog and optically dark galaxies. *Astronomy & Astrophysics*, 620:A152, 2018.
- [26] Bacon, Roland, Conseil, Simon, Mary, David, Brinchmann, Jarle, Shepherd, Martin, Akhlaghi, Mohammad, Weilbacher, Peter M., Piqueras, Laure, Wisotzki, Lutz, Lagattuta, David, Epinat, Benoit, Guerou, Adrien, Inami, Hanae, Cantalupo, Sebastiano, Courbot, Jean Baptiste, Contini, Thierry, Richard, Johan, Maseda, Michael, Bouwens, Rychard, Bouch  , Nicolas, Kollatschny, Wolfram, Schaye, Joop, Marino, Raffaella Anna, Pello, Roser, Herenz, Christian, Guideroni, Bruno, and Carollo, Marcella. The muse hubble ultra deep field survey - i. survey description, data reduction, and source detection. *A&A*, 608:A1, 2017.
- [27] Inami, H., Bacon, R., Brinchmann, J., Richard, J., Contini, T., Conseil, S., Hamer, S., Akhlaghi, M., Bouch  , N., Cl  ment, B., Desprez, G., Drake, A. B., Hashimoto, T., Leclercq, F., Maseda, M., Michel-Dansac,

- L., Paalvast, M., Tresse, L., Ventou, E., Kollatschny, W., Boogaard, L. A., Finley, H., Marino, R. A., Schaye, J., and Wisotzki, L. The muse hubble ultra deep field survey - ii. spectroscopic redshifts and comparisons to color selections of high-redshift galaxies. *A&A*, 608:A2, 2017.
- [28] Olivier Le Fèvre, G Vettolani, B Garilli, L Tresse, DBVL Bottini, V Le Brun, D Maccagni, JP Picat, R Scaramella, M Scoggio, et al. The vimos vlt deep survey-first epoch vvds-deep survey: 11 564 spectra with $17.5 \leq z \leq 24$, and the redshift distribution over $0 \leq z \leq 5$. *Astronomy & Astrophysics*, 439(3):845–862, 2005.
- [29] Dan Coe, Narciso Benítez, Sebastián F Sánchez, Myungkook Jee, Rychard Bouwens, and Holland Ford. Galaxies in the hubble ultra deep field. i. detection, multiband photometry, photometric redshifts, and morphology. *The Astronomical Journal*, 132(2):926, 2006.
- [30] Aaron M Morris, Dale D Kocevski, Jonathan R Trump, Benjamin J Weiner, Nimish P Hathi, Guillermo Barro, Tomas Dahlen, Sandra M Faber, Steven L Finkelstein, Adriano Fontana, et al. A wfc3 grism emission line redshift catalog in the goods-south field. *The Astronomical Journal*, 149(6):178, 2015.
- [31] Ivelina G Momcheva, Gabriel B Brammer, Pieter G Van Dokkum, Rosalind E Skelton, Katherine E Whitaker, Erica J Nelson, Mattia Fumagalli, Michael V Maseda, Joel Leja, Marijn Franx, et al. The 3d-hst survey: Hubble space telescope wfc3/g141 grism spectra, redshifts, and emission line measurements for 100,000 galaxies. *The Astrophysical Journal Supplement Series*, 225(2):27, 2016.
- [32] Arjen van der Wel, EF Bell, B Häussler, EJ McGrath, Yu-Yen Chang, Yicheng Guo, DH McIntosh, H-W Rix, M Barden, E Cheung, et al. Structural parameters of galaxies in candels. *The Astrophysical Journal Supplement Series*, 203(2):24, 2012.
- [33] Jorge González-López, Roberto Decarli, Ricardo Pavesi, Fabian Walter, Manuel Aravena, Chris Carilli, Leindert Boogaard, Gergö Popping, Axel Weiss, Roberto J Assef, et al. The alma spectroscopic survey in the hudf: Co emission lines and 3 mm continuum sources. *arXiv preprint arXiv:1903.09161*, 2019.
- [34] Corentin Schreiber, Maurilio Pannella, David Elbaz, Matthieu Béthermin, Hanae Inami, M Dickinson, Benjamin Magnelli, Tao

- Wang, Hervé Aussel, Emanuele Daddi, et al. The herschel view of the dominant mode of galaxy growth from $z= 4$ to the present day. *Astronomy & Astrophysics*, 575:A74, 2015.
- [35] Ryan C. Hickox, J. L. Wardlow, Ian Smail, A. D. Myers, D. M. Alexander, A. M. Swinbank, A. L. R. Danielson, J. P. Stott, S. C. Chapman, K. E. K. Coppin, J. S. Dunlop, E. Gawiser, D. Lutz, P. van der Werf, and A. Weiss. The LABOCA survey of the Extended Chandra Deep Field-South: clustering of submillimetre galaxies. *Monthly Notices of the Royal Astronomical Society*, 421(1):284–295, 03 2012.
- [36] S. D. Landy and A. S. Szalay. Bias and variance of angular correlation functions. , 412:64–71, July 1993.
- [37] Nikhil Padmanabhan, Martin White, Peder Norberg, and Cristiano Porciani. The real-space clustering of luminous red galaxies around $z \approx 0.6$: quasars in the Sloan Digital Sky Survey. *Monthly Notices of the Royal Astronomical Society*, 397(4):1862–1875, 08 2009.